HHS Public Access

Author manuscript

Gastroenterology. Author manuscript; available in PMC 2019 July 08.

Published in final edited form as:

Gastroenterology. 2018 December ; 155(6): 1852–1867. doi:10.1053/j.gastro.2018.08.041.

Loss of Tight Junction Protein Claudin-18 Promotes Rapid Cancer Development in Mouse Stomach

Susan J. Hagen[1,2], **Lay-Hong Ang**[1,2], **Yi Zheng**[1,2,6], **Salih N. Karahan**[1,7], **Jessica Wu**[1,8], **Yaoyu E. Wang**[2,3], **Tyler Caron**[1,4,9], **Aniket Gad**[1], **Sureshkumar Muthupalani**[4], and **James G. Fox**[4,5]

[1]Department of Surgery/Division of General Surgery, Beth Israel Deaconess Medical Center, Boston, MA 02215, USA

[2]Harvard Medical School, Boston, MA 02115, USA

[3]Center for Cancer Computational Biology, Dana-Farber Cancer Institute, Boston, MA 02130 USA

[4]Division of Comparative Medicine, Massachusetts Institute of Technology, Cambridge, MA 02139, USA

[5]Department of Biological Engineering, Massachusetts Institute of Technology, Cambridge, MA 02139, USA

[6]Present address: Perkin-Elmer Corporation, Hopkinton, MA 01748, USA

[7]Dr. Karahan was a visiting medical student from the Koç University School of Medicine, Bakirkoy, Istanbul,TURKEY

[8]Present address: Massachusetts Institute of Technology, Cambridge, MA 02139, USA

[9]Present address: Broad Institute, Cambridge, MA 02142, USA

Abstract

BACKGROUND & AIMS: Loss of claudin-18 (CLDN18), which is a membrane-spanning tight junction protein, is an early event associated with an aggressive phenotype and poor outcome in

Correspondence: Susan J. Hagen, Ph.D., Department of Surgery, E/RW-871, Beth Israel Deaconess Medical Center, 330 Brookline Avenue, Boston, MA 02215, Phone: (617) 667-5308, Fax: (617) 975-5562, shagen@bidmc.harvard.edu.

Author contributions:

S.J.H. conceived the overall project, did the confocal analysis, did the electron microscopy analysis, interpreted data, unraveled the genomic data, made figures, and wrote the manuscript. L.H.A. designed and performed the SIM study and did all of the immunostaining. Y.Z. designed and performed the genomic studies including Ingenunity Pathway Analysis. S.K. did most of the lineage analysis and other confocal projects for the revision. A.G. did the HIPPO signaling pathway analysis for the revision. Y.E.W. ran the RNAseq analysis and oversaw production of the final gene list. T.C. collected tissues from 2-year mice. S.M. analyzed the slides and assigned histopathology scores. J.G.F. derived and maintained the B6:129S5-CLDN18tm1Lex/Mmucd mouse colony and performed the H. pylori infection studies. Archival tissues were also collected and processed under his supervision. J.W. performed the confocal analyses in Supplementary Figure 1. J.G.F., Y.Z., L.H.A., Y.E.W, S.K., S.M., and J.W. reviewed and edited the manuscript.

Conflicts of interest

The authors disclose no conflicts of interest.

Transcript profiling:

The data discussed in this publication have been deposited in NCBI's Gene Expression Omnibus (Edgar et al., 2002) and are accessible through GEO Series accession number GSE93774 at https://www.ncbi.nlm.nih.gov/geo/query/acc.cqi?acc=GSE93774.

Writing assistance:

None

patients with gastric cancer (GC). We investigated whether CLDN18 loss also occurs in a mouse model of GC and whether CLDN18 loss, *per se*, is sufficient to drive GC development.

METHODS: Changes in CLDN18 expression were evaluated in archived tissues from B6:129 mice infected with *H. pylori* for 6–15 months. The consequence of CLDN18 loss was determined using B6:129S5-CLDN18tm1Lex/Mmucd mice, which delete *CLDN18* gene and protein expression in stomach. Tissues were analyzed by electron microscopy, histopathology, super-resolution and conventional confocal microscopy, and RNAseq.

RESULTS: Mice infected with *H. pylori* showed CLDN18 loss by 6 months post-infection that decreased over time. CLDN18, which had a basolateral rather than apical tight junction localization, was lost first from the majority of gastric glands followed by disruption and attenuation in neck and surface cells. *CLDN18*-deficient mice showed increased cellular proliferation and a molecular signature consistent with intestinalized proliferative SPEM that included defects in cellular signaling by 7 weeks after birth. By 20–30 weeks, intraepithelial neoplasia was the prominent phenotype with invasive submucosal glands and by 2-years, large and focally dysplastic polypoid tumors were present.

CONCLUSIONS: *H. pylori* infection in mice attenuates the expression of *CLDN18* early in GC development, which is similar to the results in human patients. *CLDN18* functions to regulate cell lineage differentiation and cellular signaling in the mouse stomach, without which neoplastic transformation rapidly ensues.

Keywords

Helicobacter pylori; Knockout Mice; Genomic Profile; RNAseq

Tight junction integrity in the human gastrointestinal tract is fundamental to maintain homeostasis of the host yet this is one important target of infectious and inflammatory agents. Loss of tight junction integrity is a risk factor for inflammatory bowel diseases,[1, 2] and has been identified as a major risk factor for cancer development including *H. pylori* infection-mediated GC.[3, 4] One predominant subtype of GC was recently shown to be associated with an interchromosomal translocation between claudin-18 (*CLDN18*; a tight junction protein) and Rho GTPase activating protein 26 (*ARHGAP26*; regulates actin polymerization at the plasma membrane), for which *ARHGAP* fusion to the carboxy terminus of *CLDN18* deletes its PDZ domain, and likely impairs its function.[5] This translocation was enriched in genomically stable tumors, of which 30% expressed alterations in either *RHOA* or *CLDN18*.[5] Additionally, *CLDN18* was recently identified as one of the most highly down-regulated genes in GC.[6] This gene was down-regulated in 57.5% of GC's, 73.7% of GC's with an intestinal phenotype, and in six of eight prominent GC cell lines.[6] Notably, immunostaining of intestinal-type gastric tumors showed that the attenuation of CLDN18 occurred early in the Correa cascade [7, 8] at the level of intestinal metaplasia,[6, 9] was associated with high levels of proliferation and invasion,[9, 10] and correlated with poor prognosis in GC patients.[11] In mice, Hayashi et al [12] showed that deletion of *CLDN18A2*, which is the stomach-specific isoform of *CLDN18*, resulted in atrophy and spasmolytic polypeptide-expressing metaplasia (SPEM) shortly after the onset of acid secretion due to H^+ back-diffusion and parietal cell death. However, *CLDN18A2*-deficient mice remained in a

state of atrophic gastritis/SPEM for their lifetime and did not progress to cancer.[12] Other CLDNs are also dysregulated in gastric tumors such that CLDNs, in general, are viewed as a contributor to GC pathogenesis owing to their specific association with outcome parameters in human patients.[4] There is a lack, however, of experimental data to support a role for CLDNs in cancer pathogenesis.

Recent studies demonstrated significant changes in gene expression in the lung and bone of *CLDN18*-deficient mice (*CLDN18*DM),[13, 14] accompanied by abnormalities in the stomach including high gastric pH and a decrease in the number of parietal cells.[15] Because human GC patients downregulate both *CLDN18A1* (lung-specific isoform) and *CLDN18A2*, not just the stomach isoform,[6, 9] we assessed the association of *CLDN18* and *H. pylori* on GC pathogenesis using infected mice deficient in *CLDN18*. We aimed to test the hypothesis that without *CLDN18*, *H. pylori*-mediated GC pathogenesis would be accelerated. Instead, we found that cancer develops rapidly in *CLDN18*DM with or without infection.

Materials and Methods

Mice

*CLDN18*DM (*CLDN18−/−*; B6:129S5/SvEvBrd background[14]) were purchased as frozen embryos from the MMRRC (University of California at Davis) and re-derived, bred, and housed at MIT in an AAALAC International approved facility. Equal numbers of male and female mice were used at 7 and 10 weeks after birth. Because no differences were found in the results from male or female mice, the data were pooled. The stomach from male mice at 2-years after birth was also evaluated. Animal experiments were performed according to institutional guidelines and the animal protocol was approved by the Committee on Animal Care at MIT.

H. pylori Infection and Colonization

*CLDN18*DM, wild-type (WT; *CLDN*18+/+; B6:129S5/SvEvBrd), and heterozygous (*CLDN*18+/−; B6:129S5/SvEvBrd background) mice were infected with *H. pylori* SS1[16] or PMSS1[17] at 6-weeks as described,[18] and tissues collected for analysis at 20 and 30 weeks post-infection. Control mice were sham-infected as described previously.[18] Colonization was verified by qPCR as described previously.[19]

Histological Preparation and Analysis of Stomach Histopathology

Archival tissues from B6:129 mice sham- or infected with *H. pylori* at 6, 12, or 15 months post infection [20] were used for the experiments in Figures 1 and 2. For the remainder of experiments, tissues from *CLDN18*DM and litter-matched control mice were embedded in paraffin, sectioned, and then stained with H&E or with Alican Blue (pH 2.5) and Periodic Acid Schiff (PAS). For histopathology, tissues were scored by a board certified Veterinary Pathologist (SM) without foreknowledge of source. Sections were photographed using an Axioimager microscope system (Carl Zeiss).

Confocal Microscopy, Structured Illumination Microscopy (SIM), and Image Analysis

Antibodies used for immunostaining of paraffin sections with antigen retrieval methods and dilutions are listed in Supplementary Table 1. For confocal microscopy, sections were mounted in Vectashield (Vector Labs) containing DAPI and for SIM, the sections were mounted in 2, 2'-thiodiethanol (TDE) reagent (Sigma-Aldrich) containing Dabco 33-LV (Sigma-Aldrich). Tissues were evaluated using an LSM880 confocal system (Carl Zeiss) or an Elyra super-resolution microscope system (Carl Zeiss). For confocal studies, the images for individual experiments were collected on the same day with the same microscope settings and analyzed with Volocity software (PerkinElmer). SIM was used to collect 3-color 3-D stacks, which were aligned using Image J Fuji software. The aligned images were visualized in 3-D using Volocity software.

Electron Microscopy

Tissues from *CLDN18*DM were processed for electron microscopy as described [21] but without vascular perfusion. Analysis was performed on a JEOL1400 electron microscope outfitted with Orius CCD cameras (Gatan).

RNA Preparation and RNASeq

Laser capture microdissection, using a PALM Laser Capture Microdissection System (Carl Zeiss), was used to capture tissue from the neck region of WT (male, n=3) or *CLDN18*DM (male, n=3) at 7 weeks after birth. Purified RNA was submitted to the Dana-Farber Center for Cancer Computational Biology.

RNA quantity was determined on the Qubit using the RNA Assay Kit (ThermoFisher Scientific) and RNA quality was determined on the Bioanalyzer using the RNA Pico Kit (Agilent). A library was prepared using the NEBNext Ultra RNA Library Prep Kit for Illumina (New England Biolabs, Inc). RNAseq was performed using a HiSeq2000 sequencing system (Illumina), with a paired-end 51 cycle kit. The resulting sequences were mapped to the Mouse genome (mm10) using STAR aliger (http://bioinformatics.oxfordjournals.org/content/early/2012/10/25/bioinformatics.bts635), quantified by feature Counts (http://www.ncbi.nlm.nih.gov/pubmed/24227677), and analyzed using DESeq (http://www.ncbi.nlm.nih.gov/pubmed/20979621) for differential expression. *P*-values were adjusted by the Benjamini-Hochberg procedure. [22] IPA was done using Ingenuity software (Qiagen), accessed through Harvard Medical School.

To identify genes with significant expression changes and for IPA, we chose those genes with a Log2 ≥ 2 (positive or negative), with an adjusted *P*-value of 0.0001 or less. These stringent cut-off parameters yielded 672 differentially expressed genes for comparison.

Statistical Analyses

Data were analyzed by one- or two-way ANOVA using SigmaPlot 10 software (Systat Software). ANOVA on ranks was preformed if variances were not equal. Graphs were produced in the same software. Significance was set at $*P < 0.05$, $**P < 0.01$, or $***P < 0.001$; NS, not significantly different.

Results

Attenuation of CLDN18 Expression Occurs in H. pylori Infected Mice

CLDN18 was highly expressed in surface and gland epithelial cells from archived tissues (Figure 1). In contrast, CLDN18 was attenuated or lost altogether in tissues from *H. pylori* infected mice (Figure 2). By 6 months post-infection, about 70% of gastric glands were negative for CLDN18 (Figure 2A and E) and at 15 months post-infection, where the gastric histopathology had progressed to intraepithelial neoplasia,[20] CLDN18 expression was lost in more than 80% of gastric glands (Figure 2E). We also noted a reduction in the intensity of CLDN18 expression in *H. pylori*-infected mice that was accompanied by the attenuation and disruption of CLDN18 in neck-region cells (Figure 2B and E). One notable feature of CLDN18 in control tissues, which was discovered by using super-resolution microscopy techniques, was that CLDN18 is not part of the tight junction complex but rather is expressed along the basolateral membrane (Figure 1E). CLDN18 formed a dense, basket-like structure along the basolateral membrane in surface (not shown), neck, and base epithelial cells from sham-infected mice (Figure 1E). By contrast, the basal expression of CLDN18 was absent, localization along the lateral membrane was patchy, and there was a considerable gap between the tight junction complex and CLDN18 in cells from *H. pylori*-infected mice (Figure 2F). The base of gastric glands in *H. pylori*-infected mice, in those cells with remaining CLDN18 expression, had no organized localization of this protein along the basolateral membrane (Figure 2C and F). The antibody used for this study recognized *CLDN18A1* in lung and *CLDN18A2* in stomach (Figure 1 and 2D), suggesting that both CLDN18 isoforms are down-regulated in *H. pylori* infected mice. CLDN18 in surface epithelial cells was not significantly attenuated until 15 months post-infection (Figure 2E). These results support the hypothesis that *H. pylori* infection in mice results in the focal loss, attenuation, and disruption of CLDN18 in gastric epithelial cells.

Targeted Deletion of CLDN18 Results in the Development of Pre-neoplastic Stomach Lesions in Mice by 7 Weeks after Birth

We first confirmed by immunostaining that *CLDN18*DM do not express CLDN18A1 or CLDN18A2 in stomach (Supplementary Figure 1A).

In the stomach, surface epithelial cells from *CLDN18*DM had a tattered appearance, and the neck and base regions contained glands with metaplastic cells (Figure 3A and B). Surface and pit epithelial cells from control tissues had PAS and *Ulex europaeus* agglutinin 1 (UEA1)-positive mucus whereas the same region in *CLDN18*DM had only a sparse mucous layer (Figure 3C and D and Supplementary Figure 2A). PAS and UEA1 were also present along the length of gastric glands to the base in *CLDN18*DM (Figure 3D and E and Supplementary Figure 2A and C). Alcian blue stained cells were present at the gland base (Figure 3E), which also contained cells co-expressing the SPEM markers *Griffonia simplicifolia* (GSII) lectin and gastric intrinsic factor (GIF; Supplementary Figure 2F).

To quantify the morphological defects in *CLDN18*DM compared to WT or heterozygous mice at 7–10 weeks after birth (Figure 3F), we used the murine gastric histopathology scoring paradigm.[23] For all categories evaluated, histopathology scores for heterozygous

mice were nearly identical to WT mice. Robust corpus atrophy scores for *CLDN18*DM (Figure 3F) were confirmed by immunostaining (Supplementary Figure 1B-D), which demonstrated nearly complete parietal and chief cells loss in *CLDN18*DM by 7 weeks after birth. Additionally, there was increasing dysplasia including gland distortion, branching, pleomorphism, and stratification of the epithelium (Figure 3F). Epithelial defects in *CLDN18*DM included frequent dilated glands and large areas of rounded surface epithelial cells that resembled “tattering”. Inflammation also increased from 7 to 10 weeks in *CLDN18*DM (Figure 3F). Pseudopyloric metaplasia, which we defined as antralization of gastric glands in the corpus,[23] and foveolar hyperplasia were prominent in tissues from *CLDN18*DM (Figure 3F).

Proliferating cells, which are Ki67 positive, localized to the isthmus region in tissues from WT mice but were greatly expanded to include the length of gastric glands in tissues from *CLDN18*DM (Figure 4A). In fact, the total number of epithelial cells increased by 56.1% and the number of Ki67-positive proliferating cells increased by 638.1% in *CLDN18*DM compared to WT mice (Figure 4 and Supplementary Figure 5C). In *CLDN18*DM, proliferating cells in the neck region expressed the foveolar lineage marker UEA1 while some cells in the gland base were also positive (Supplementary Figure 2A and C). Cells in the neck and base also expressed the SPEM lineage marker GSII, and some cells in both regions co-expressed the SPEM marker GSII and the foveolar marker UEA1 (Supplementary Figure 2B, D, and F and Figure 5E). Some cells co-expressed the SPEM markers GSII and GIF in addition to Ki67 (Supplementary Figure 2D), and the intestinal marker CFTR (Supplementary Figure 3B), suggesting they are intestinalized proliferative SPEM.[24, 25] Thus, the high gastric histopathology activity index (GHAI) score (Figure 3F) in addition to lectin and other specific marker staining patterns supported that pre-neoplastic lesions were present in the stomach of *CLDN18*DM by 7 weeks.

Potential mechanisms that drive this unusually high level of proliferation in *CLDN18*DM were investigated. Although changes in β-catenin localization from lateral membranes to the nucleus would be the most logical process,[26, 27] there were few clearly visible changes in localization of this protein at 7 weeks (Supplementary Figure 4). Nonetheless, β-catenin/WNT downstream effectors including CD44 and the ephrin receptor, EPHB2, were highly upregulated (Figure 7D), suggesting increased transcriptional activity. CD44, a stem cell marker that regulates proliferation in stomach,[28, 29] was localized to the isthmus region in WT mice but was localized to the gland base in *CLDN18*DM, where some CD44+ cells co-localized with proliferating cells expressing Ki67 (Figure 4B). Ephrin (EFN) and ephrin receptor (EPH) expression, markers that are associated with proliferative activity in stem/progenitor and cancer cells,[30] was also significantly different in WT vs *CLDN18*DM (Figure 4C and D and Supplementary Table 2). In particular, EFNB1/B2 and EPHB2 gene expression were significantly upregulated (Supplementary Table 2 and Figure 7D) with EFNB1/B2 and EPHB2 localized to apical and basolateral compartments, respectively, in WT mice but along the basolateral membrane of all cells in *CLDN18*DM (Figure 4C and D). Similar to CD44+ cells, some proliferative, Ki67+ cells, co-localized with EFNB1/B2 or EPHB2 in the surface and base while all proliferative cells in the isthmus and neck regions co-localized with these markers in tissues from *CLDN18DM* (not shown). Lastly, the Yes-associated protein 1 (YAP1)/HIPPO signaling pathway, which also regulates cell

proliferation,[31] was upregulated and activated in *CLDN18*DM (Figure 5A and B). Activated YAP1 in WT mice localized to parietal and neck cells, with minimal localization to chief or surface cells (Figure 5C and Supplemental Figure 5A). By contrast, activated YAP1 localized to metaplastic cells in the pit, neck and base regions in *CLDN18*DM (Figure 5D), where it co-localized with UEA1+ cells in the neck region but was excluded from UEA1+, GSII+, or UEA1/GSII+ co-positive cells at the gland base (Figure 5E). Cells expressing activated YAP1 also co-localized with the proliferation marker Ki67 in *CLDN18*DM (Supplementary Figure 5). Our results show that cell proliferation in *CLDN18*DM at 7 weeks is extensive and may be regulated by different pathways that are simultaneously co-expressed in the mucosa.

Targeted Deletion of CLDN18 Results in the Formation of Gastric Tumors

To explore the idea that *CLDN18* deficiency drives cancer development, we examined stomach histopathology from *CLDN18*DM at 20 and 30 weeks post-sham or *H. pylori* infection and at 2 years (Figure 6A–E and Supplementary Figure 6). In *H. pylori* infected mice, mean histopathology scores were similar for WT and $CLDN18^{+/-}$ mice (Supplementary Figure 6), irrespective of *H. pylori* strain (data for the PMSS1 strain is not shown). However, data for *CLDN18*DM were nearly identical despite infection status (Supplementary Figure 6). Because this was an unexpected finding, we evaluated the colonization of *H. pylori* in *CLDN18*DM by qPCR and found none. These results suggest that *H. pylori* are unable to colonize the stomach of *CLDN18DM*.

At 20 weeks post sham-infection, there were eight notable features of the mucosa: 1) the entire corpus was affected rather than patchy areas of clonal cancer formation (not shown); 2) inflammation, foveolar hyperplasia, and epithelial defects were extensive; 3) there was nearly complete atrophy of the gastric corpus; 4) the tissue architecture was consistent with high grade dysplasia/gastrointestinal intraepithelial neoplasia,[23] which also resembled intramucosal carcinoma in humans [32, 33]. Cells lining gastric pits, particularly the stratified areas, were not stratified squamous epithelium but resembled subtype II or subtype III granule-free cells (gastric stem cells); [34] 5) the neck region had the most extensive desmoplasia and in some, but not all tissues, contained small glands budding-out into the lamina propria consistent with an early invasive phenotype. By electron microscopy, the epithelial cells most closely resembled precursor (stem) cells from the neck or zymogenic lineages; [34, 35] 6) the base of gastric glands was highly distorted and irregular. By electron microscopy, endocrine and caveolated (tuft) cells were more numerous, while the epithelial cells had small granules with a dense core, apical cytoplasm that appeared to bleb and pinch-off large structures into the gastric lumen; 7) there was extensive exfoliation of epithelial cells into the gland lumen, often forming cyst-like structures that contained exfoliated cells; and 8) pseudopyloric metaplasia was extensive in tissues from uninfected or infected *CLDN18*DM and was of a much higher grade than in WT mice infected with *H. pylori*. GHAI scores at 20 and 30 weeks post sham- or *H. pylori* infection support the extensive, rapid, and aggressive nature of mucosal changes that occur in *CLDN18*DM with or without *H. pylori* infection.

By 2-years after birth, the stomach of *CLDN18*DM contained polypoid tumors with focal high grade dysplasia occupying approximately 85% of the glandular epithelium (Figure 6F). At 30 weeks after sham or *H. pylori* infection, invasive glands [23] were present in the submucosa near lymphatic vessels that had cells within the lumen (Supplementary Figure 7A). By 2 years, these invasive glands were additionally noted in the serosal layer of the stomach (Figure 6F), and had an elongated and asymmetrical appearance, stromal hyperplasia, loss of nuclear polarity and nuclear crowding, and an invasive-seeming leading edge (Figure 6F). Invasive glands at both 30 weeks and 2-years contained epithelial cells that were UEA1+, GSII+ or UEA1/GSII+ but had few proliferative (Ki67+) cells (Supplementary Figure 7B). Despite the formation of large tumors, invasive glands in the serosa, and the suggestion of cancer cells in the lymphatics, there was no metastatic population to lymph nodes or other organs by 2 years after birth (not shown). This finding is consistent with other GC models in mice.[23, 25]

To determine mechanisms responsible for mucosal changes in *CLDN18*DM, we compared the transcriptome of *CLDN18*-deficient vs WT mice at 7 weeks after birth. We chose 7 weeks to analyze because inflammation scores (WT vs heterozygous vs *CLDN18*DM) were not significantly different at this time (Figure 3F). While *CLDN18*DM significantly up-regulated IL-1α and −1β gene expression (Figure 7A), gene expression for interleukin-1 receptor antagonist (*IL-1RN*) was also highly up-regulated (Figure 7E). This result suggests that there is likely suppression of IL-1biological activity by the concomitant expression of the receptor antagonist. Additionally, no change in gene expression for *TNFA* (TNF-α) or *IFNG* (IFN-γ), IL-6/gp130, MIP-2 (*CXCL2*) (Figure 7A), or IL-12, IL-27, IL-13, IL-17, IL-18, or IL-23 (Supplementary Table 3) were present in *CLDN18*DM. IL-8 functional homologues *KC* (*CXCL1*) and *LIX* (*CXCL5*) showed an increase in expression (Figure 7A), suggesting neutrophil recruitment and activation. *CXCR1*, the receptor for IL-8 homologs in mice, was highly down-regulated (Figure 7A), suggesting that Il8-like function may also be attenuated. Of particular interest was the increase in expression of *IL33* and its receptor *IL1RL1* in *CLDN18*DM at 7 weeks (Figure 7A). Despite this result, gene expression of macrophage and other immune cell markers recently linked to IL-33 expression [36] were not increased nor were key M1 or M2 polarization markers [24, 37] except for SOCS3 (Supplementary Table 3). However, activated *SOCS3*-expressing macrophages co-express the M1 marker iNOS (*NOS2*)[38], which is not upregulated in *CLDN18*DM (Supplementary Table 3). Overall, the results suggest that changes in histopathology and gene expression at 7 weeks are not the result of IL-33 expression or macrophage recruitment or polarization.

Identification of Factors in CLDN18DM that Regulate the Mucosal Transition to Gastric Cancer- Genomic Markers for Metaplasia and Dysplasia

Consistent with the histopathology data, differentiated cell markers for gastric epithelial cells were significantly reduced in the gene panel (Figure 7B). Ten markers specific for SPEM were identified in C57/BL6 mice infected with *Helicobacter felis* [39] of which prothymosin-α (*PTMA*; +1.03, $p=1.26E^{-05}$), growth arrest-specific 5 (*GAS5*; +1.12; $p=9.67E^{-06}$), and NOP56 ribonuclear protein (*NOP56*; +0.84, $p=1.27\ E^{-03}$) were significantly upregulated in *CLDN18*DM. Numerous markers associated with the emergence of SPEM from acute parietal cell loss in C57/BL6 mice [40] were also upregulated in

*CLDN18*DM (Figure 7B and Supplementary Table 4). From fifty putative markers of metaplastic progression that were identified as highly up-regulated in cultured gastric cells, [41] we identified twenty that were also up-regulated in *CLDN18*DM (Supplementary Table 4). Some of the noted pan-SPEM and acute SPEM markers [42, 43] were also up-regulated in *CLDN18*DM (Figure 7B and Supplementary Table 4). Because SPEM lineages in mice acquire intestinal characteristics in the presence of inflammation,[42] a process required for GC progression, we evaluated gene expression of these markers in *CLDN18*DM (Figure 7B and Supplementary Table 4). Most notable was the up-regulation of *CFTR*, which localized to the apical surface of SPEM cells in the neck and base (Supplementary Figure 3B), and *DMBT1* (Figure 7B). While some markers identified as specific to SPEM with inflammation[42] were up-regulated in *CLDN18*DM, all of the markers identified in SPEM with chronic inflammation [42] were highly up-regulated (Supplementary Table 4). All of the markers for SPEM with chronic inflammation in our study were also identified in human metaplasia of the stomach.[44] Kras, which leads to metaplastic lineage transitions in GC development,[43] was also up-regulated at 7 weeks in *CLDN18*DM (+0.79, $p = 2.9\ E^{-03}$). The human dysplasia marker urokinase plasminogen activator (*PLAUR*), identified in invasive tumors,[32] was highly up-regulated (Figure 7B). These results demonstrate that *CLDN18*DM at 7 weeks have robust expression of metaplasia and dysplasia markers that are also found in human GC.

Top Regulator Effect Networks

We next determined that four upstream regulators of gene expression could be attributed to the dataset of differentially regulated genes (Figure 7C). Peroxisome proliferator-activated receptor (PPAR)-gamma (*PPARG*), PPAR-delta (*PPARD*), and PPAR-gamma co-activator 1 alpha (*PPARGC1A*) regulate lipid metabolism, which is one of the most significantly altered pathways in the neck region of *CLDN18*DM (Figure 7C). As such, some of the most highly down-regulated genes in the neck region attributed to lipid metabolism (Figure 7E). These results are consistent with Mills et al,[45] who showed that gastric parietal cells express numerous genes dedicated to fatty acid absorption and synthesis, β-oxidation, and mitochondrial transport. *CSF2* is a cytokine that controls granulocyte and macrophage development. Its predicted activation is consistent with the landscape of increasing inflammation in *CLDN18*DM.

Although *TRP53* gene expression increased in *CLDN18*DM (Figure 7C), IPA analysis suggests that this regulator is inhibited in relationship to its numerous downstream effectors. Because p53 target gene expression is consistent with the down-regulation of p53, we evaluated the expression of its conserved intracellular inhibitor, inhibitor of apoptosis-stimulating protein of p53 (*PPP1R13L*), which was significantly up-regulated in *CLDN18*DM (+1.49; $p = 1.65E^{-05}$). Alternatively, functional mutations in p53 may be present in *CLDN18*DM by 7 weeks. Overall, IPA pathway analysis suggests that the pathway abnormalities in *CLDN18*DM at 7 weeks most relevant to GC pathogenesis may be those in the p53 pathway while other top regulator pathways reflect the high level of gastric atrophy in *CLDN18*DM.

Gastric and Cancer Stem Cells

To explore the identity of metaplastic cells in the neck region, we examined gene expression levels for normal and cancer stem cells, as well as ligands that direct their differentiation (Figure 7D). The expression of genes for gastric stem cells including *TNFRSF19* (Troy) and markers enriched in Troy$^+$ stem cells including *LGR5, LGR1, RNF43,* and *ZNRF3* [46] were unchanged in *CLDN18*DM (Figure 7D). *ASCL2*, the Achaete-scute family bHLH transcription factor, also enriched in Troy$^+$ stem cells [46], was upregulated in *CLDN18*DM (Figure 7D). In contrast, gene expression for surface markers enriched in cancer stem cells increased in *CLDN18*DM (Figure 7D), with the localization of *EPHB2, CD44*, and *VIL1* confirmed by immunostaining (Figure 4B–D and Supplementary Figure 8). Of particular interest, villin (*VIL1*) localized to *DCLK1*-expressing tuft (caveolated) cells (Supplementary Figure 8). Because WNT target genes *AUXIN2*, *EPHB2*, *CD44*, *APC*, and *TCF3* (+1.81, p = 2.4 E^{-14}), in addition to cyclin D1 (*CCND1*; +1.34, p = 6.96 E^{-06}), MMP-9 (*MMP9*; +5.28, p = 1.62 E^{-07}), PPAR-delta (Figure 7C), and gastrin (*GAST*; Figure 7B), increased in *CLDN18*DM, we evaluated gene expression of Wnt pathway effectors. Our database indicates that Wnt 9a and 16, which are specific for epithelial progenitors in the stomach,[47] were downregulated, but the non-canonical WNT signaling pathway effectors 5a and 11 were highly upregulated (Figure 7D). The up-regulation of gene expression for non-canonical Wnt signaling receptors *ROR2* (+2.93, p = 1.72 E^{-17}) additionally support the idea that non-canonical Wnt activation occurs in these mice. We also noted an upregulation of differentiation pathways typically limited to the stem cell compartment but highly upregulated in the gastric neck region of *CLDN18*DM. In particular, Notch pathway effectors, including *NOTCH 4* and *DLL4* (Figure 7D), and JAG1 (+1.013, p = 7.8 E^{-04}), the later of which is a c-Wnt pathway target. We also determined that one set of Notch-induced transcriptional repressors, *HEY1* (−1.54, p = 0.0074) and *HEY2* (−1.44, p = 0.048) were down-regulated in *CLDN18*DM. These results suggest that *CLDN18*DM at 7 weeks repress constitutive WNT but activate non-canonical WNT signaling, which are effectors that link WNT and Notch pathways, and significantly up-regulate markers for cancer stem cells.

The most highly up- and down-regulated genes in *CLDN18*DM were involucrin (*IVL*) and acidic mammalian chitinase (AMCase, *CHIA*), respectively (Figure 7E). Involucrin, which is a component of the keratinocyte, is highly expressed in the mouse forestomach but not in the corpus. In *CLDN18*DM, this marker may be associated with desmoplasia or some other aspect of the developing neoplasia. AMCase is highly expressed in the mouse corpus,[48] with normalized counts similar to the β subunit of the H$^+$, K$^+$-ATPase (not shown). AMCase was recently identified as the second most highly expressed gene in the human corpus compared to antrum and a gene showing the strongest down-regulation in patients with *H. pylori*-induced gastric atrophy.[49] Many of the highly up-regulated genes from the list of top 10 molecules are STAT5a or STAT3 downstream effectors, including involucrin, *MMP10*, *CLDN2*, *MUC4*, and *IL1RN*.

Discussion

Tight junctions are required for the maintenance of epithelial barrier function and mucosal homeostasis but are often dysregulated in disease. Emerging evidence suggests that a

relationship exists between CLDN expression and cancer development and progression in most epithelial cancers,[50] but their role in disease pathogenesis remains unknown. Our results showed that *H. pylori* infection attenuates *CLDN18* expression in mice, and that the deletion of *CLDN18* in stomach results in progressive changes in mucosal architecture that lead to gastrointestinal intraepithelial neoplasia and tumorigenesis. These results suggest that *H. pylori* infection itself and/or inflammation are required to attenuate *CLDN18* expression but once CLDN18 is lost, cancer progression can occur independently. Whether tight junction barrier function is disrupted in *CLDN18*DM, and what role this plays in GC pathogenesis is unknown.

CLDN18 is described as a protein localized to the apical tight junction complex;[12] our study suggests that it is rather a basolateral membrane protein. In the stomach, other CLDNS also localize to the basolateral membrane, including CLDNS 3 and 5, while CLDN 4 localizes specifically to the apical tight junction complex.[51] Although classical tight junction complexes have not been shown on the basolateral membrane of epithelial cells, Claude and Goodenough [52] identified discontinuous tight junction strands along the basolateral membrane of stomach epithelial cells by freeze fracture microscopy. It is thus possible that the basket-like, discontinuous localization of CLDN18 along the basolateral membrane that we demonstrate by super-resolution techniques correlates to those putative tight junction-like structures. Although it is not clear what function these structures might have along the basolateral membrane, they may be required to limit cation transport by forming a series of cation-selective pores along the basolateral membrane, or some other important function, like creating a scaffold for cell signaling pathway effectors.[53]

Our results differ from those recently demonstrated for *CLDN18A2*-deficient mice.[12] One important difference was that *CLDN18A2*-deficient mice expressed high levels of the lung variant 1, *CLDN18A1,* which localized to tight junctions.[12] Having tight junction associated *CLDN18* may protect the mucosa and additionally compensate for one or more important functions lacking in the *CLDN18* variant 1 and 2-deficient mice we studied. Understanding functional differences between tight junction-associated vs basolateral claudins will be important to determine why the absence of basolateral *CLDN18* promotes cancer development.

High rates of cellular proliferation occur in *CLDN18*DM, which is similar to the mucosal response to *H. pylori* infection. Numerous pathways are linked to the proliferative response in *H. pylori*-mediated GC, including β-catenin,[26, 27] CD44 (variant 9),[28, 54] EFNB/EPHB receptor signaling,[55, 56] and HIPPO signaling.[57, 58] Individually, these pathways can be attributed to tumorigenesis in GC patients, and can be associated with patient outcome or survival. Although subtle changes in β-catenin localization occurred in *CLDN18DM* at 7 weeks, the downstream effectors CD44, EFNB1 and B2, and EPHB2 were highly upregulated. CD44 may predominantly drive proliferation at the base of gastric glands where it is most highly expressed whereas EFNB½/EPHB2 signaling may drive proliferation along the entire mucosa. Proliferation regulated by HIPPO/YAP1 signaling is likely prominent in the pit and neck with a minor role at the gland base. The expression of other markers linked to *H. pylori*-induced proliferation may also be involved in the proliferative response in *CLDN18*DM, including gastrin and Indian hedgehog.[59] Additionally, there was a significant

decrease in the receptor for bone morphogenetic factor, *BMPR1* (−2.86, p = 4.45E^{-24}), which typically reduces proliferation by regulating signaling.[60] Thus, the proliferative response in *CLDN18*DM at 7 weeks is highly complicated with participants from numerous different pathways.

Genomic markers of GC progression in mice have been evolving over time and have resulted in the identification of important gene footprints to distinguish different steps in the Correa cascade.[40–42] Inflammation is known to drive GC pathogenesis,[61] resulting in an increase in specific transcripts that appear to be consistently expressed in different models. Although we chose the 7 week time point to analyze because inflammation was limited in *CLDN18*DM, the gene expression signature in these mice was consistent with SPEM during chronic inflammation.[42] This inflammation-induced signature could have been driven by increased levels of Il-33, although immune effectors specific for the IL-33 response [36, 62] were mostly down-regulated in *CLDN18*DM making this an unlikely option. Likewise, macrophage markers,[36] including those that promote SPEM after parietal cell loss,[24] were mostly down-regulated in *CLDN18*DM at 7 weeks suggesting this pathway also plays little role in the initial phenotype. Wnt and Notch pathway effectors, but particularly cancer stem cells, may be important for dysregulation of tissue homeostasis in our mice. This profile includes cells highly expressing ephrin receptor 2B, CD44, SOX2, and villin. Villin is a tuft cell marker in GI epithelium{Höfer, 1992 1585 /id} that we show accounts for the constitutive expression of villin in mouse stomach. Tuft cells increase in number after parietal cell loss,[64] which may explain why *VIL1* expression is highly upregulated and the localization of DCLK1-positive, villin-positive tuft cells greatly expand in our atrophic *CLDN18*DM. Tuft cells are closely associated with SPEM and repopulate the mucosa close to proliferating metaplastic and dysplastic cells.[65] Furthermore, this population of cells was recently shown to secrete acetylcholine, which induces the secretion of nerve growth factor from gastric epithelial cells resulting in neuron expansion and tumorigenesis.[66] This cholinergic signaling also promotes the activation of YAP1,[66] which may explain why YAP1 activation and robust cellular proliferation occur in our model.

In summary, we describe an important role for CLDN18 in stomach by using an *in vivo* genetic approach in mice. Our data demonstrates that CLDN18 supports mucosal homeostasis and is a major tumor suppressor in mice. Conversely, in the absence of *CLDN18*, changes in mucosal architecture, cellular transformation, and invasive properties occur that are consistent with cancer development. Because the down-regulation of *CLDN18* expression is correlated with worse clinical outcome in advanced GC patients, determining the specific pathways regulated by *CLDN18* may serve as important new therapeutic targets for the treatment of this disease.

Supplementary Material

Refer to Web version on PubMed Central for supplementary material.

Acknowledgements

We would like to acknowledge Dr. Blanca Piazuelo (Vanderbilt University, Nashville, TN) for assisting with the tissue histopathology analysis; Drs. David Alpers (Washington University, St. Louis MO) and Dr. Seth Alper (Beth

Israel Deaconess Medical Center, Boston, MA) for the anti-GIF and anti-SLC4A antibodies, respectively; and Dr. Doug Richardson (Harvard Center for Biological Imaging) for assistance and training on the super-resolution microscope systems.

Funding

The authors would like to acknowledge past and ongoing support for this work: Harvard Catalyst | The Harvard Clinical and Translational Science Center, National Center for Research Resources and the National Center for Advancing Translational Sciences, National Institutes of Health (NIH) Award 1UL1 TR001102–01 and financial contributions from Harvard University and its affiliated academic health care centers, Department of Surgery Bridge funds, and NIH grant P30 DK034854 (S.J.H.); NIH grants R01 CA093405, P30 ES002109, R01OD011141, and P01CA028842 (J.G.F.); and a Research Science Institute/Center for Excellence in Education Summer Research Fellowship (J.W.)

Abbreviations used in this paper:

AB	Alcian Blue
CLDN	Claudin
CLDN18	Claudin-18 protein expression
CLDN18	Claudin-18 gene expression
CLDN18A1	lung-specific isoform of CLDN18
CLDN18A2	stomach-specific isoform of CLDN18
CLDN18DM	Claudin-18 deficient mice
EFN	Ephrin
EPH	Ephrin receptor
GC	Gastric cancer
GHAI	Gastric histopathology activity index
GIF	Gastric intrinsic factor
GSII	Lectin from Griffonia simplicifolia used to identify mucous neck/ SPEM cells in the stomach
H&E	Hematoxylin and eosin
H. pylori	Helicobacter pylori
IPA	Ingenuity Pathway Analysis
PAS	Periodic-acid Schiff
SIM	Structured illumination (super-resolution) microscopy
SPEM	Spasmolytic polypeptide-expressing metaplasia
UEA-1	Lectin from Ulex europaeus agglutinin 1 used to identify foveolar cells in the stomach

WT	Wild-type mice
YAP1	Yes-associated protein 1
ZO-1	Zonula occludins-1

References

1. Weber CR, Nalle SC, Tretiakova M, et al. Claudin-1 and claudin-2 expression is elevated in inflammatory bowel disease and may contribute to early neoplastic transformation. Lab Invest 2008;88:1110–1120. [PubMed: 18711353]
2. Clayburgh DR, Shen L, Turner JR. A porus defense: the leaky epithelial barrier in intestinal disease. Lab Invest 2004;84:282–291. [PubMed: 14767487]
3. Wroblewski LE, Peek RM, Wilson KT. Helicobacter pylori and gastric cancer: factors that modulate disease risk. Clin Microbiol Rev 2010;23:713–739. [PubMed: 20930071]
4. Caron TJ, Scott KE, Fox JG, et al. Tight junction disruption: Helicobacter pylori and dysregulation of the gastric mucosal barrier. World J Gastroenterol 2015;21:11411–11427. [PubMed: 26523106]
5. Bass AJ, Thorsson V, Shmulevich ITCGARN. Comprehensive molecular characterization of gastric adenocarcinoma. Nature 2014;513:202–209. [PubMed: 25079317]
6. Sanada Y, Oue N, Mitani Y, et al. Down-regulation of the claudin-18 gene, identified through serial analysis of gene expression data analysis, in gastric cancer with an intestinal phenotype. J Pathol 2006;208:633–642. [PubMed: 16435283]
7. Correa P Human gastric carcinogenesis: a multistep and multifactorial process- First American Cancer Society Award Lecture on Cancer Epidemiology and Prevention. Cancer Res 1992;52:6735–6740. [PubMed: 1458460]
8. Correa P, Houghton J. Carcinogenesis of Helicobacter pylori. Gastroenterology 2007;133:659–672. [PubMed: 17681184]
9. Matsuda Y, Semba S, Ueda J, et al. Gastric and intestinal claudin expression at the invasive front of gastric carcinoma. Cancer Sci 2007;98:1014–1019. [PubMed: 17459057]
10. Oshima T, Shan J, Okugawa T, et al. Down-regulation of claudin-18 is associated with the proliferative and invasive potential of gastric cancer at the invasive front. PLoS ONE 2013;8:e74757.
11. Jun K-H, Kim J-H, Jung J-H, et al. Expression of claudin-7 and loss of claudin-18 correlate with poor prognosis in gastric cancer. Int J Surg 2014;12:156–162. [PubMed: 24333468]
12. Hayashi D, Tamura A, Tanaka H, et al. Deficiency of claudin-18 causes paracellular H^+ leakage, up-regulation of interleukin-1-beta, and atrophic gastritis in mice. Gastroenterology 2012;142:292–304. [PubMed: 22079592]
13. Li G, Floodby P, Luo J, et al. Knockout mice reveal key roles foor claudin 18 in alveolar barrier properties and fluid homeostasis. Am J Respir Cell Mol Biol 2014;51:210–222. [PubMed: 24588076]
14. Linares GR, Bommage R, Powell DR, et al. Claudin 18 is a novel negative regulator of bone resorption and osteoclast differentiation. J Bone Miner Res 2012;27:1553–1565. [PubMed: 22437732]
15. Alshbool FZ, Alarcon C, Wergedal JE, et al. A high-calcium diet failed to rescue an osteopenia phenotype in claudin-18 knockout mice. Physiol Rep 2014;2:e00200.
16. Lee A, O'Rourke J, DeUngria MC, Robertson B, Daskalopoulos G, Dixon MF. A standardized mouse model of Helicobacter pylori infection: Introducing the Sydney strain. Gastroenterology 1997;112:1386–1397. [PubMed: 9098027]
17. Arnold I, Lee JY, Amieva MR, et al. Tolerance rather than immunity protects from Helicobacter pylori-induced gastric preneoplasia. Gastroenterology 2011;140:199–209. [PubMed: 20600031]
18. Hagen SJ, Ohtani M, Zhou J-R, et al. Inflammation and foveolar hyperplasia are reduced by supplemental dietary glutamine during Helicobacter pylori infection in mice. J Nutr 2009;139:912–918. [PubMed: 19261732]

19. Fox JG, Wang TC, Robers AB, et al. Host and microbial constituents influence Helicobacter pylori-induced cancer in a murine model of hypergastrinaemia. Gastroenterology 2003;124:1879–1890. [PubMed: 12806621]
20. Rogers AB, Taylor NS, Whary MT, et al. Helicobacter pylori but not high salt induces gastric intraepithelial neoplasia in B6129 mice. Cancer Res 2005;65:10709–10715. [PubMed: 16322215]
21. Karam SM, Leblond CP. Identifying and counting epithelial cell types in the “corpus” of the mouse stomach. Anat Rec 1992;232:231–246. [PubMed: 1546802]
22. Benjamini Y, Hochberg Y. Controlling the false discovery rate: a practical and powerful approach to multiple testing. J R Statist Soc B 1995;57:289–300.
23. Rogers AB. Histologic scoring of gastritis and gastric cancer in mouse models. Methods Mol Biol 2012;921:189–203. [PubMed: 23015505]
24. Petersen CP, Weis VG, Nam KT, et al. Macrophages promote progression of spasmolytic polypeptide-expressing metaplasia following acute loss of parietal cells. Gastroenterology 2014;146:1727–1738. [PubMed: 24534633]
25. Petersen CP, Mills JC, Goldenring JR. Murine models of gastric corpus preneoplasia. Cell Mol Gastroenterol Hepatol 2017;3:11–26. [PubMed: 28174755]
26. Franco AT, Israel DA, Washington MK, et al. Activation of β-catenin by carcinogenic Helicobacter pylori. Proc Natl Acad Sci USA 2011;102:10646–10651.
27. Nagy TA, Wroblewski LE, Wang D, et al. β-catenin and p120 mediate PPARδ-dependent proliferation induced by Helicobacter pylori in human and rodent epithelia. Gastroenterology 2011;141:553–564. [PubMed: 21704622]
28. Khurana SS, Riehl TE, Moore BD, et al. The hyaluronic acid receptor CD44 coordinates normal and metaplastic epithelial progenitor cell proliferation. J Biol Chem 2013;288:16085–16097. [PubMed: 23589310]
29. Takaishi S, Okumura T, Tu S, et al. Identification of gastric cancer stem cells using the cell surface marker CD44. Stem Cells 2010;27:1006–1020.
30. Genander M, Halford MM, Xu N-J, et al. Disassociation of Eph2B signaling pathways mediating progenitor cell proliferation and tumor suppresion. Cell 2019;139:679–692.
31. Patel SH, Camargo FD, Yimlamai D. Hippo signaling in the liver regulates organ size, cell fate, and carcinogenesis. Gastroenterology 2017;152:533–545. [PubMed: 28003097]
32. Correa P, Piazuelo BM. The gastric precancerous cascade. J Dig Dis 2012;13:2–9. [PubMed: 22188910]
33. Piazuelo BM, Correa P. Gastric cancer: Overview. Colomb Med (Cali) 2013;44:192–201. [PubMed: 24892619]
34. Karem SM, Leblond CP. Dynamics of epithelial cells in the corpus of the mouse stomach I. Identification of proliferative cell types and pinpointing of the stem cells. Anat Rec 1993;236:259–279. [PubMed: 8338232]
35. Karem SM, Leblond CP. Dynamics of epithelial cells in the corpus of the mouse stomach III. Inward migration of neck cells followed by progressive transformation into zymogenic cells. Anat Rec 1993;236:297–313. [PubMed: 8338234]
36. Buzzelli JN, Chalinor HV, Pavlic DI, et al. IL33 is a stomach alarmin that initiates a skewed Th2 response to injury and infection. Cell Mol Gastroenterol Hepatol 2015;1:203–221. [PubMed: 28210674]
37. Barros MHM, Hauck F, Dreyer JH, et al. Macrophage polarization: an immunohistochemical approach for identifying M1 and M2 macrophages. PLoS ONE 2013;8:e80908.
38. Wilson HM. SOCS proteins in macrophage polarization and function. Front Immunol 2014;5:00357.
39. Nomura S, Baxter T, Yamaguchi H, et al. Spasmolytic polypeptide-expressing metaplasia to preneoplasia in H. felis-infected mice. Gastroenterology 2004;127:582–594. [PubMed: 15300590]
40. Nozaki K, Ogawa M, Williams JA, et al. A molecular signature of gastric metaplasia arising in response to acute parietal cell loss. Gastroenterology 2008;134:511–522. [PubMed: 18242217]

41. Weis VG, Petersen CP, Mills JC, et al. Establishment of novel in vivo mouse chief cell and SPEM cultures identifies MAL2 as a marker oof metaplasia in the stomach. Am J Physiol Gastrointest Liver Physiol 2014;307:G792.
42. Weis VG, Sousa JF, Lafleur BJ, et al. Heterogeneity in mouse SPEM lineages identifies markers of metaplastic progression. Gut 2013;62:1270–1279. [PubMed: 22773549]
43. Choi E, Hendley AM, Bailey JM, et al. Expression of activated Ras in gastric chief cells of mice leads to the full spectrum of metaplastic lineage transitions. Gastroenterology 2016;150:918–930. [PubMed: 26677984]
44. Lee H-J, Nam KT, Park HS, et al. Gene expression profiling of metaplastic lineages identifies CDH17 as a prognostic morker in early-stage gastric cancer. Gastroenterology 2010;139:213–225. [PubMed: 20398667]
45. Mills JC, Syder AJ, Hong CV, et al. A molecular profile of the mouse gastric parietal cell with and without exposure to Helicobacter pylori. Proc Natl Acad Sci USA 2001;98:13687–13692. [PubMed: 11717430]
46. Stange DE, Koo B-K, Huch M, et al. Differentiated Troy^{+} chief cells act as reserve stem cells to generate all lineages of the stomach epithelium. Cell 2013;155:357–368. [PubMed: 24120136]
47. Giannakis M, Stappenbeck TS, Mills JC, et al. Molecular properties of adult mouse gastric and intestinal epithelial progenitors in their niches. J Biol Chem 2006;281:11292–11300. [PubMed: 16464855]
48. Ohno M, Togashi Y, Tsuda K, et al. Quantification of chitinase mRNA levels in human and mouse tissues by real-time PCR: species-specific expression of acidic mammalian chitinase in stomach tissues. PLoS ONE 2013;8:e67399.
49. Nookaew I, Thorell K, Worah K, et al. Transcriptome signatures in Helicobacter pylori-infected mucosa identifies acidic mammalian chitinase loss as a corpus atrophy marker. BMC Med Genomics 2013;6:41. [PubMed: 24119614]
50. Singh AB, Dhawan P. Claudins and cancer: fall of the soldiers entrusted to protect the gate and keep the barrier intact. Semin Cell Dev Biol 2015;42:58–65. [PubMed: 26025580]
51. Rahner C, Mitic LL, Anderson JM. Heterogeneity in expression and subcellular localization of claudins 2, 3, 4, and 5 in the rat liver, pancreas and gut. Gastroenterology 2001;120:411–423. [PubMed: 11159882]
52. Claude P, Goodenough DA. Fracture faces of zonulae occludentes from “tight” and “leaky” epithelia. J Cell Biol 1973;58:390–400. [PubMed: 4199658]
53. Hagen SJ. Non-canonical functions of claudin proteins: Beyone the regulation of cell-cell adhesions. Tissue Barriers 2017;5:e1327839.
54. Initiation Zavros Y. and maintanance of gastric cancer: a focus on CD44 variant isoforms and cancer stem cells. Cell Mol Gastroenterol Hepatol 2017;4:55–63. [PubMed: 28560289]
55. Uchiyama Y, Saeki N, Ogawa K. Aberrant EpB/ephrin-B expression in experimental gastric lesions and tumor cells. World J Gastroenterol 2015;21:453–464. [PubMed: 25593460]
56. Wong SS, Kim K-M, Ting JC, et al. Genomic landscape and genetic heterogeneity in gastric adenocarcinoma revealed by whole-genome sequencing. Nat Commun 2014;5:5477. [PubMed: 25407104]
57. Ma L-G, Bian S-B, Cui J-X, et al. LKB1 inhibits the proliferation of gastric cancer cells by suppressing the nuclear localization of Yap and β-catenin. Int J Mol Med 2016;37:1039–1048. [PubMed: 26936013]
58. Jiao S, Wang H, Shi Z, et al. A peptide mimicking VGLL4 function acts as a YAP antagonist therapy against gastric cancer. Cancer Cell 2014;25:166–180. [PubMed: 24525233]
59. Feng R, Aihara E, Kenny S, et al. Indian hedgehog mediates gastrin-induced proliferation in stomach of adult mice. Gastroenterology 2014;147:655–666. [PubMed: 24859162]
60. Todisco A Regulation of gastric metaplasia, dysplasia, and neoplasia by bone morphogenic protein signaling. Cell Mol Gastroenterol Hepatol 2017;3:339–347. [PubMed: 28462376]
61. Fox JG, Wang TC. Inflammation, atrophy, and gastric cancer. J Clin Invest 2007;117:60–69. [PubMed: 17200707]

62. Schmitz J, Owyang A, Oldham E, et al. IL-33, an interleukin-1-like cytokine that signals via the IL-1 receptor-related protein ST-2 and induces T helper type 2-associated cytokines. Immunity 2005;23:479–490. [PubMed: 16286016]

63. Höfer D, Drenckhahn D. Identification of brush cells in the alimentary and respiratory system by antibodies to villin and fimbrin. Histochemistry 1992;98:237–242. [PubMed: 1459863]

64. Choi E, Petersen CP, Lapierre LA, et al. Dynamic expansion of gastric mucosal doublecortin-like kinase 1-expresssing cells in response to parietal cell loss is regulated by gastrin. Am J Pathol 2015;185:2219–2231. [PubMed: 26073039]

65. Kikuchi M, Nagata H, Watanabe N, et al. Altered expression of a putative progenitor cell marker DCAMKL1 in the rat gastric mucosa in regeneration, metaplasia, and dysplasia. BMC Gastroenterology 2010;10:65. [PubMed: 20565818]

66. Hayakawa Y, Sakitani K, Konishi M, et al. Nerve growth factor promotes gastric tumorigenesis through aberrant cholinergic signaling. Cancer Cell 2017;31:21–34. [PubMed: 27989802]

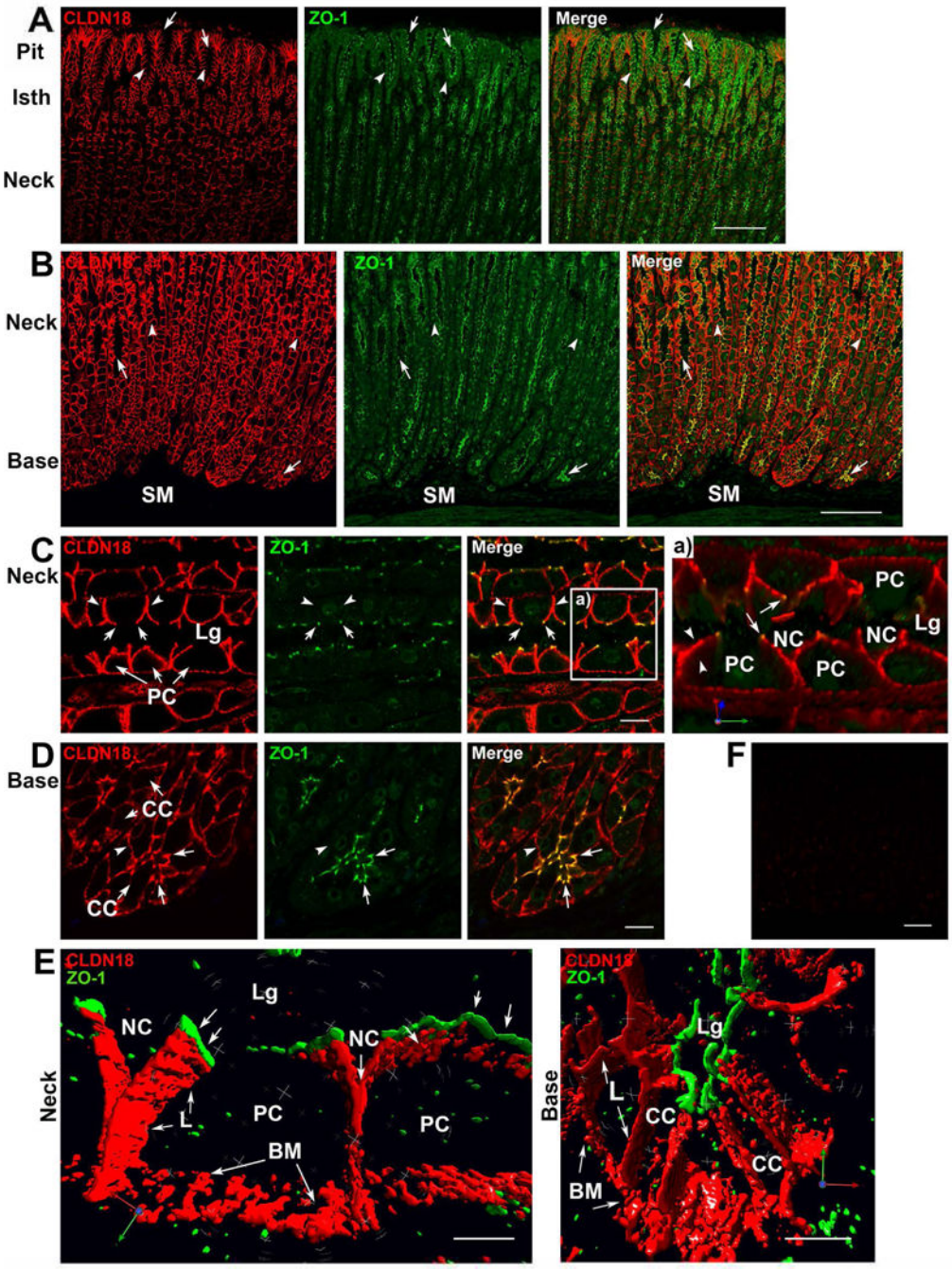

Figure 1.

CLDN18 localized to the basolateral membrane in tissues from sham-infected B6:129 mice at 6 months post- infection.[20] Data were the same at 12 and 15 months post-infection, which served as a control for the results in Figure 2E. (*A, B*) Localization of CLDN18 and ZO-1 in the pit/isthmus/neck (*A*) or in the neck/base (*B*) by confocal microscopy. *Scale bars*: 100 μm. (*C-D*) Higher magnification confocal images of CLDN18 and ZO-1 in the neck region (*C*) or the gland base (*D*). *Scale bars*: 100 μm. (*a*) Projected image of CLDN18 and ZO-1 from multiple z-stacked images. (*E*) Localization of CLDN18 in parietal cells (Neck) or

chief cells (Base) taken by super-resolution, structured illumination microscopy. *Scale bars*: 5 μm. (*F*) Negative control for CLDN18 staining; anti-CLDN18 antibody containing its blocking peptide. *Scale bar*: 10 μm. For panels *A*-*E*: BM, basolateral membrane; CC; chief cells; L, lateral cell membrane (also denoted by arrowheads in low magnification images); Lg, lumen of a gastric gland; NC, Neck mucous cell; PC, parietal cell; SM, submucosa; arrows, tight junctions.

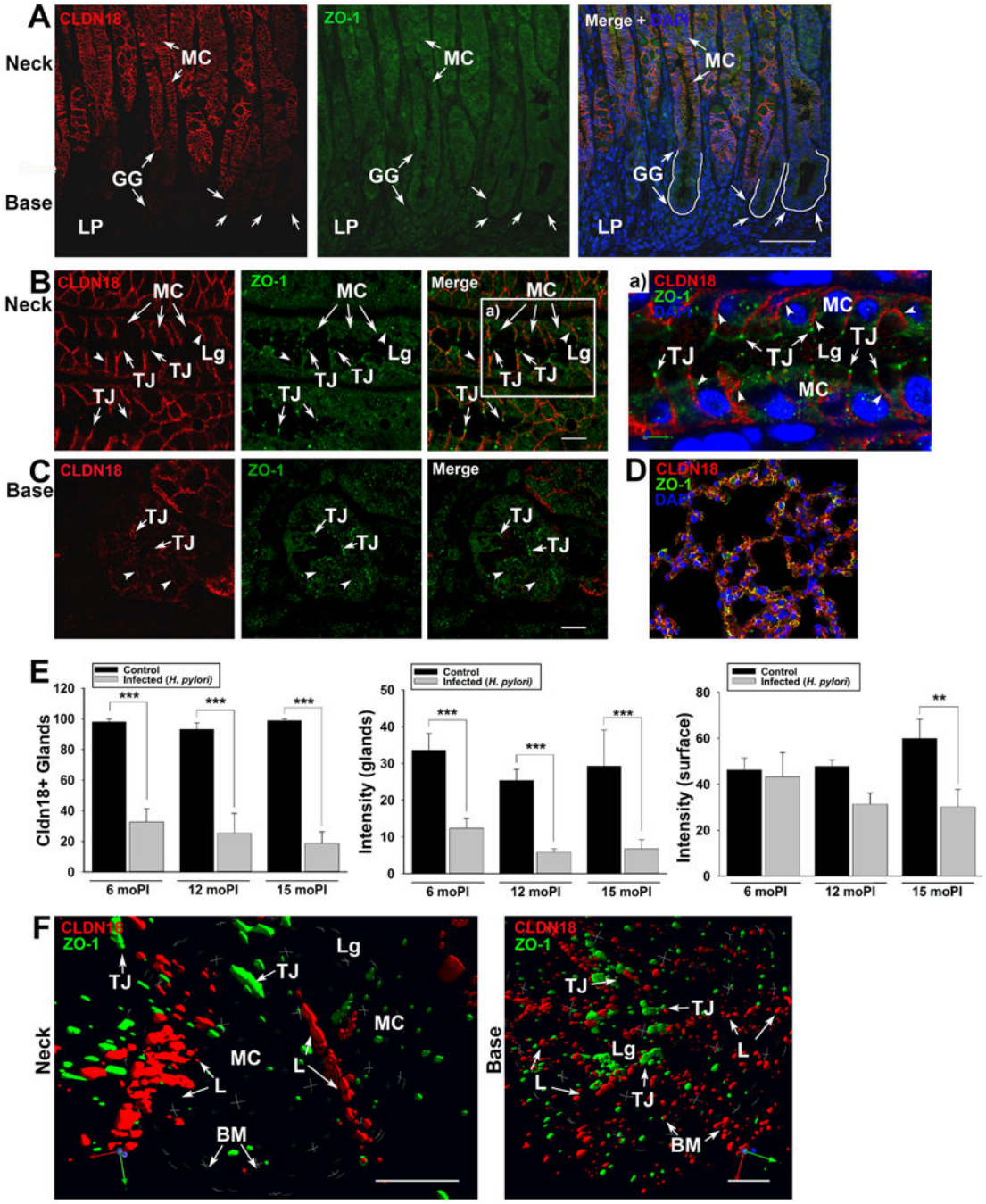

Figure 2.

CLDN18 is disrupted and attenuated in tissues from *H. pylori* infected B6:129 mice. Images are from 6 months post-infection. (*A*) Expression of CLDN18 and ZO-1 in the neck and gland base. Arrows and the solid line indicate the position of gastric glands. *Scale bar*: 100 μm. (*B-C*) Higher magnification images of CLDN18 and ZO-1, with or without DAPI stain, in the neck region (*B*) or the gland base (*C*). *Scale bar* (*B*): 10 μm; (*C*), 50 μm. (*a*) Projected image of CLDN18 and ZO-1from multiple z-stacked images in the neck region. (*D*) Localization of CLDN18 in lung tissues, confirming that the antibody used for our studies

also recognized CLDN18 variant 1 (lung variant). (*E*) Quantification of CLDN18 expression in sham (Control)- or *H. pylori*-infected mice from 6 to 15 months post-infection. Error bars mark SEM from 10–15 mice per treatment and per time point. (*F*) Super-resolution SIM images of the neck region and gland base of tissues from 12-month *H. pylori* infected mice. The red stippling in Figure 2*F* is background due to low levels of CLDN18 expression. *Scale bars*: 5 μM. For panels *A*-*F*: BM, basolateral membrane; GG, gastric glands; L, lateral cell membrane (also denoted as arrowheads in low magnification images); Lg, lumen of a gastric gland; LP, lamina propria; MC, metaplastic epithelial cell; TJ, tight junction.

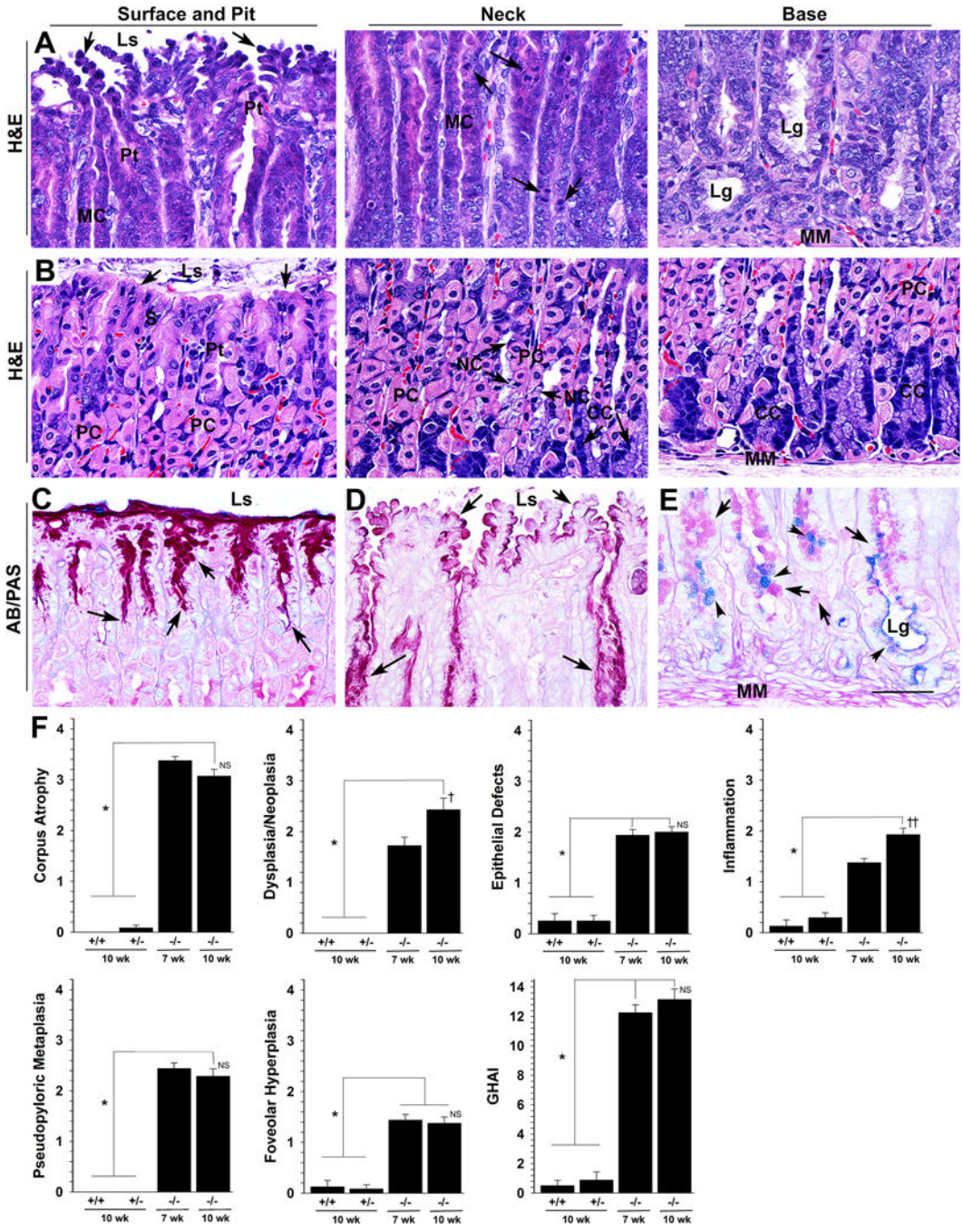

Figure 3.

Pre-malignant lesions are prominent in the stomach of *CLDN18*DM by 7 weeks after birth. (*A, B*) H&E stained tissues of the surface and pit, neck, or base of gastric glands from *CLDN18*DM (*A*) or WT (*B*) mice. (*C, D*) Images of surface epithelial cells from WT (*C*) or *CLDN18*DM (*D*) mice stained with Alcian Blue (AB)/Periodic Acid Schiff (PAS) to identify the mucous layer. Arrows, PAS positive mucous (purple). (*E*) Base of gastric glands from *CLDN18*DM stained with AB/PAS to identify mucous. Arrows, PAS positive mucous (purple); arrowheads, AB positive mucous (blue). For panels *A*-*E* unless noted otherwise:

CC, chief (zymogenic) cells; Ls, lumen of the stomach; Lg, lumen of a gastric gland; MC, metaplastic epithelial cell; MM, muscularis mucosa; N, neck mucous cell; PC, parietal cells; Pt, gastric pit; arrows, proliferating cells. *Scale bar* (in *E* for *A*-*E*): 200 μm. (*F*) Histopathology scores (0–4) for WT (+/+), heterozygous (+/−), or *CLDN18*DM (−/−) mice at 7 and 10 weeks after birth. Gastric histopathology activity index (GHAI) represents the sum of individual histopathology scores for each group. There was no infection with *H. pylori* in these mice. In all panels, * compared to heterozygous and WT mice at 10 weeks; †, or ††, $P < 0.05$ or 0.01, respectively, compared to *CLDN18*DM at 7 weeks; NS, no significant difference; error bars mark SEM for 10–12 mice per treatment and per time point.

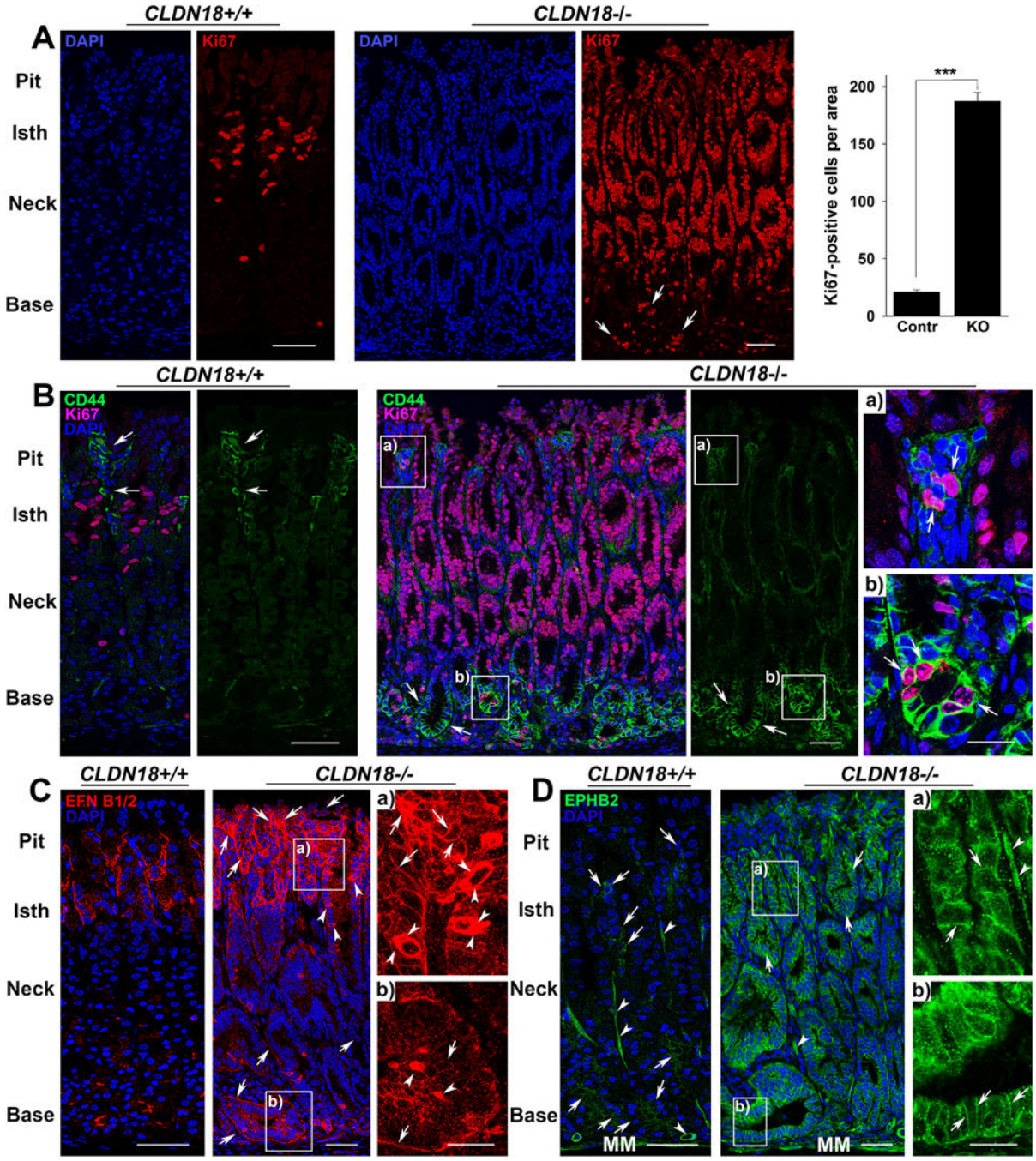

Figure 4.

Proliferation increased in the stomach of *CLDN18*DM; a subset of Ki67+ proliferating cells co-localized with CD44 or with ephrin B1/B2 and the ephrin receptor B2 at 7 weeks. (*A*) Quantification of Ki67-positive proliferating cells in WT (*CLDN*18+/+) vs *CLDN18*DM (*CLDN18*−/−). *Scale bars*: 50 μm. In the graph, area measurements were normalized to 50 mm^2. Error bars mark SEM from 3 male and 3 female mice (pooled) per treatment and per time point. (*B*) Co-labeling of Ki67+ proliferating cells with CD44 (arrows) in WT (*CLDN*18+/+) and *CLDN18*DM (*CLDN18*−/−). *Scale bars*: 50 μm. (*a*, *b*) Higher

magnification images from the boxed regions in *B*. Arrows indicate Ki67+/CD44+ cells in the neck (*a*) or gland base (*b*) of *CLDN18*DM. Nuclei in proliferating cells are pink due to the co-localization of Ki67 (red) with DAPI (blue). *Scale bar*: 20 μm. (*C*) Ephrin (EFN)B1/B2 expression in WT (*CLDN18*+/+) vs CLDN18DM (*CLDN*18−/−). *Scale bars*: 50 μm. (*a*, *b*) Higher magnification images from the boxed regions in *C*. While EFNB1/B2 is membrane-associated in most cells (arrows), there is also an intracellular localization (arrowheads) in some cells at the surface (*a*) and in the gland base (*b*). *Scale bar*: 20 μm. (*D*) Ephrin receptor (EPH)B2 expression in WT (*CLDN18*+/+) vs *CLDN18*DM (*CLDN18*−/−). EPHB2 is also expressed in smooth muscle cells of the muscularis mucosa (MM), which extend into the lamina propria (arrowheads). *Scale bars*: 50 μm. (*a*, *b*) Higher magnification images from the boxed regions in *D*. Arrows indicate the basolateral membrane localization of EPHB2 in cells of the pit (*a*) or gland base (*b*) that co-localize with Ki67+ proliferating cells. *Scale bar*: 20 μm.

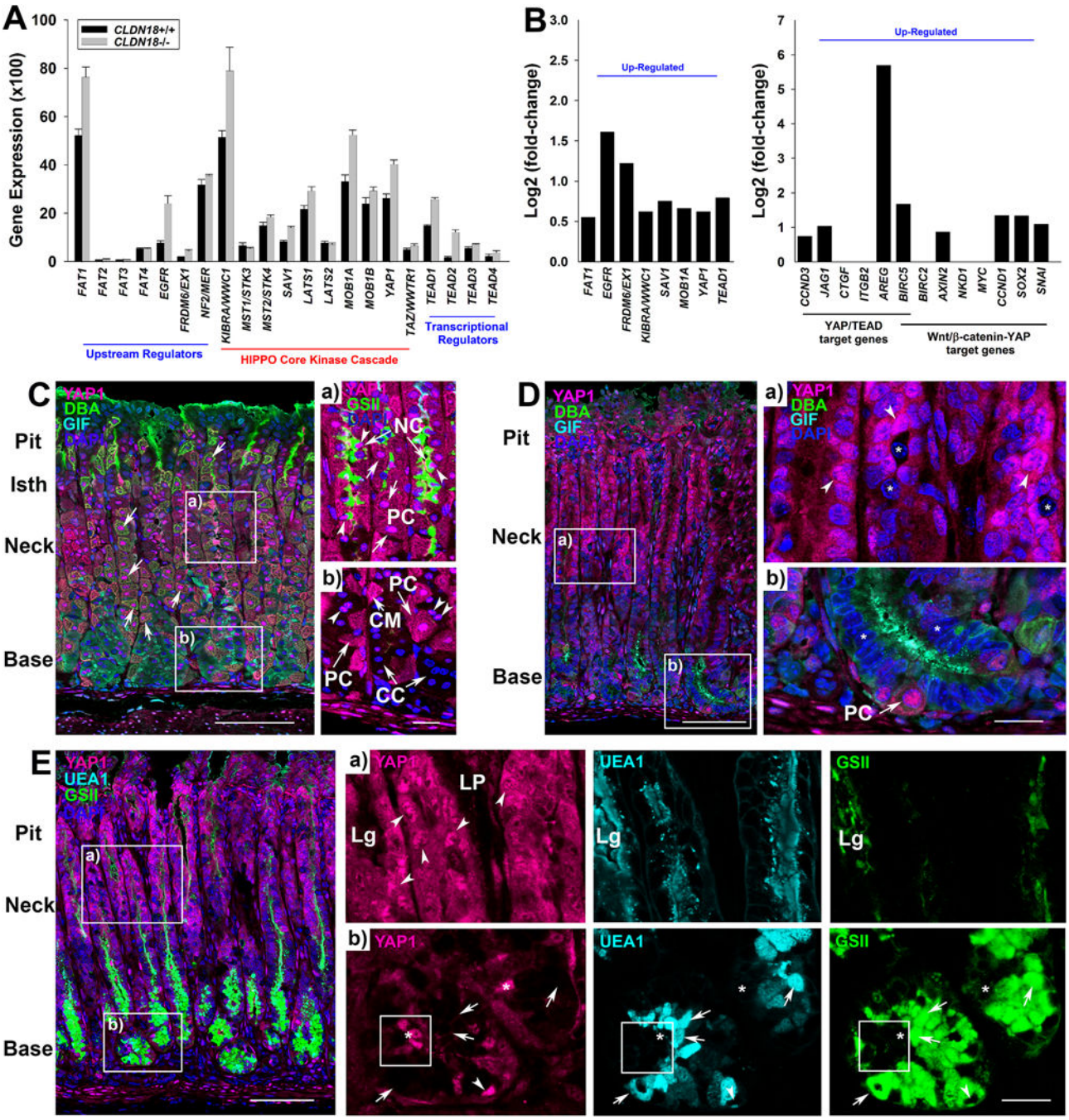

Figure 5.

Yes-associated protein 1 (YAP1)/HIPPO signaling is activated in *CLDN18*DM. (*A*) Normalized counts (mean) for effectors that regulate HIPPO signaling from WT (*CLDN18*+/+) or *CLDN18*DM (*CLDN18*−/−). Error bars mark SEM from 3 mice per treatment. (*B*) Fold-change for those regulators in *A* that are significantly up-regulated (*P*-value of 0.05 or less) in WT vs *CLDN18*DM including downstream YAP/TEAD and Wnt/β-catenin-YAP target genes. When no bar is descripted, there was no significant gene fold-change between WT and *CLDN18*DM. Data are from 3 mice (male) per treatment. (*C*)

Localization of activated YAP1in tissues from WT mice. *Scale bar*: 100 μm. (*a,b*) In control tissues, activated YAP1 localized to DBA+ parietal cells (arrows) and GSII+ neck cells (arrowheads) with little expression in GIF+ chief cells. CC; chief cells; NC, neck cell; PC, parietal cell. *Scale bar*: 20 μm. (*D*) Localization of activated YAP1in tissues from *CLDN18*DM. *Scale bar*: 100 μm. (*a, b*) Activated YAP1 localized to metaplastic cells (arrowheads) in tissues from *CLDN18*DM but is excluded from DBA+/GIF+ cells at the base of gastric glands (*). Some cells in the neck are also negative for YAP1 (*). PC; parietal cell. *Scale bar*: 20 μm. (*E*) Co-localization of activated YAP1 with the foveolar lineage marker UEA1 and the SPEM lineage marker GSII in tissues from *CLDN18*DM. *Scale bar*: 100 μm. (*a, b*) YAP1+ cells (arrowheads) in the neck also express UEA1 and some co-express GSII but YAP1+ cells in the gland base (*) do not express either lineage marker. Lg; lumen of a gastric gland; LP, lamina propria. *Scale bar*: 20 μm.

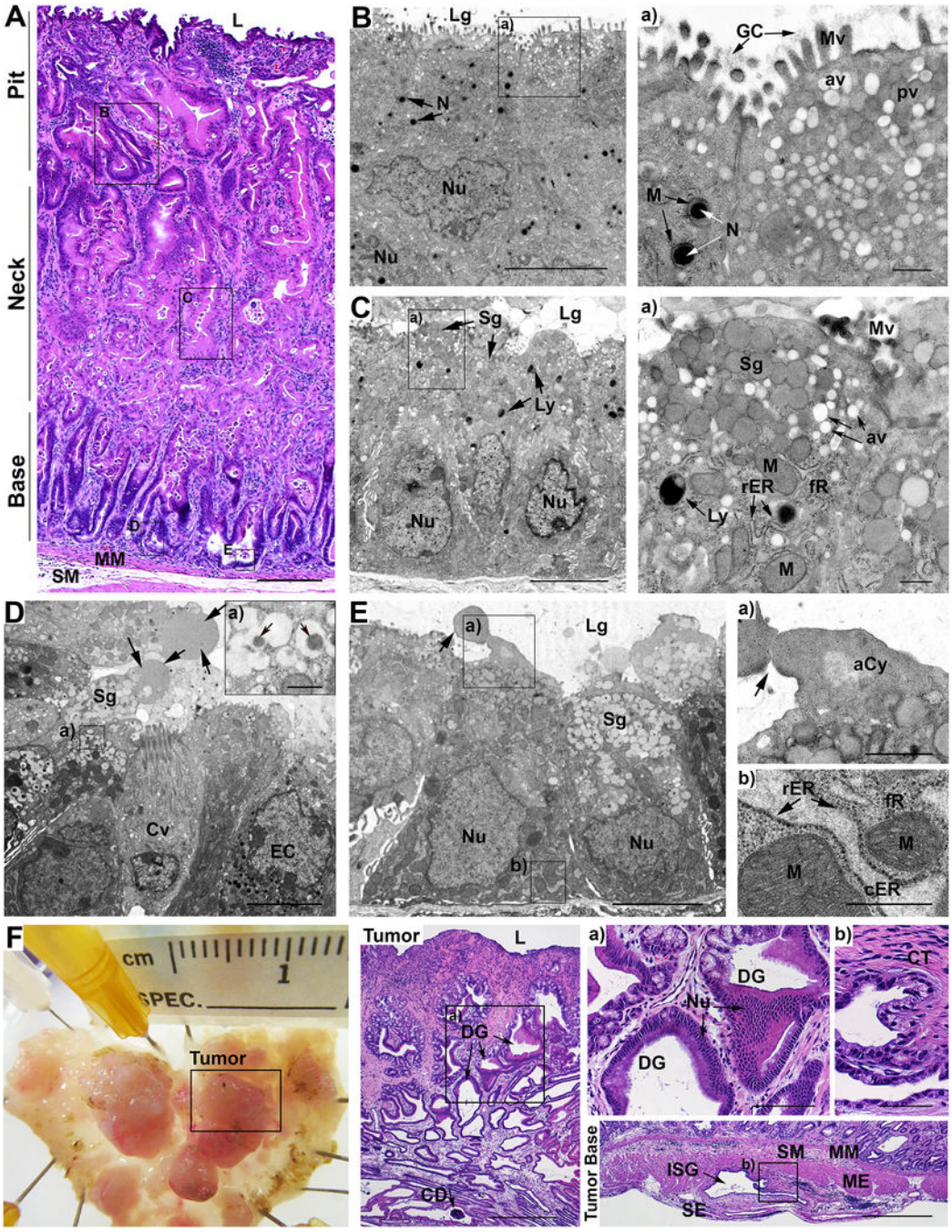

Figure 6.

*CLDN18*DM progress to intraepithelial neoplasia by 20 weeks post sham-infection and have large pollipoid tumors at 2 years. (*A*) H&E stained section of the stomach at 20 weeks post sham-infection. *Scale bar*: 200 μm. (*B*) Electron micrograph from the boxed area; pit region in Figure 6*A*. *Scale bar*: 5 μm. a) Cells in this region resembled subtype II or subtype III granule-free cells (gastric stem cells). *Scale bar*: 0.5 μm. (*C*) Electron micrograph from the boxed area; neck region in Figure 6*A*. *Scale bar*: 5 μm. a) Cells in this region resembled precursor (stem) cells from the neck or zymogenic lineages. *Scale bar*: 0.5 μm. (*D*) Electron

micrograph from the boxed area; gland base region in Figure 6*A*. Endocrine and caveolated (tuft) cells were numerous. *Scale bar*: 5 μm. a) Epithelial cells in this region had small granules with a dense core. *Scale bar*: 0.5 μm. (*E*) Electron micrograph from the boxed area; gland base region in Figure 6*A*. *Scale bar*: 5 μm. a) The apical cytoplasm of most epithelial cells appeared to bleb and pinch-off large structures into the gastric lumen. *Scale bar*: 1 μm. b) The base of epithelial cells had extensive and dilated rough endoplasmic reticulum, and large mitochondria with extensive cristae. *Scale bar*: 0.5 μm. (*F*) Stomach from *CLDN18*DM (male) at 2-years. Tumors were large, and in H&E sections were focally dysplastic. *Scale bar:* 500 μm. a) Higher magnification images of dysplastic glands within the tumor parenchyma. *Scale bar:* 100 μm. At the tumor base, asymmetrical invasive lesions were present in the serosal layer. *Scale bar:* 500 μm. b) Stromal hyperplasia, loss of nuclear polarity, and nuclear crowding, occurred in the invasive glands. *Scale bar:* 50 μm. In panels *A-F* unless noted otherwise: aCy, apical cytoplasmic blebs; av, apical vesicles; cER, dilated cisternae of the ER; Cv, caveolated cells; CD, calcium deposit; CT, connective tissue; DG, dysplastic glands; EC, endocrine cells; fR, free ribosomes; GC, glycocalyx; ISG, invasive gland; L, gastric lumen; Ly, lysosomes; Lg, lumen of gastric glands; M, mitochondria (with or without nodules, N); ME, muscularis externa; MM, muscularis mucosa; Mv, microvilli;; Nu, nuclei; pv, pre-secretory vesicles; rER, rough endoplasmic reticulum; SM, submucosa; SE, serosa; Sg, secretory granules.

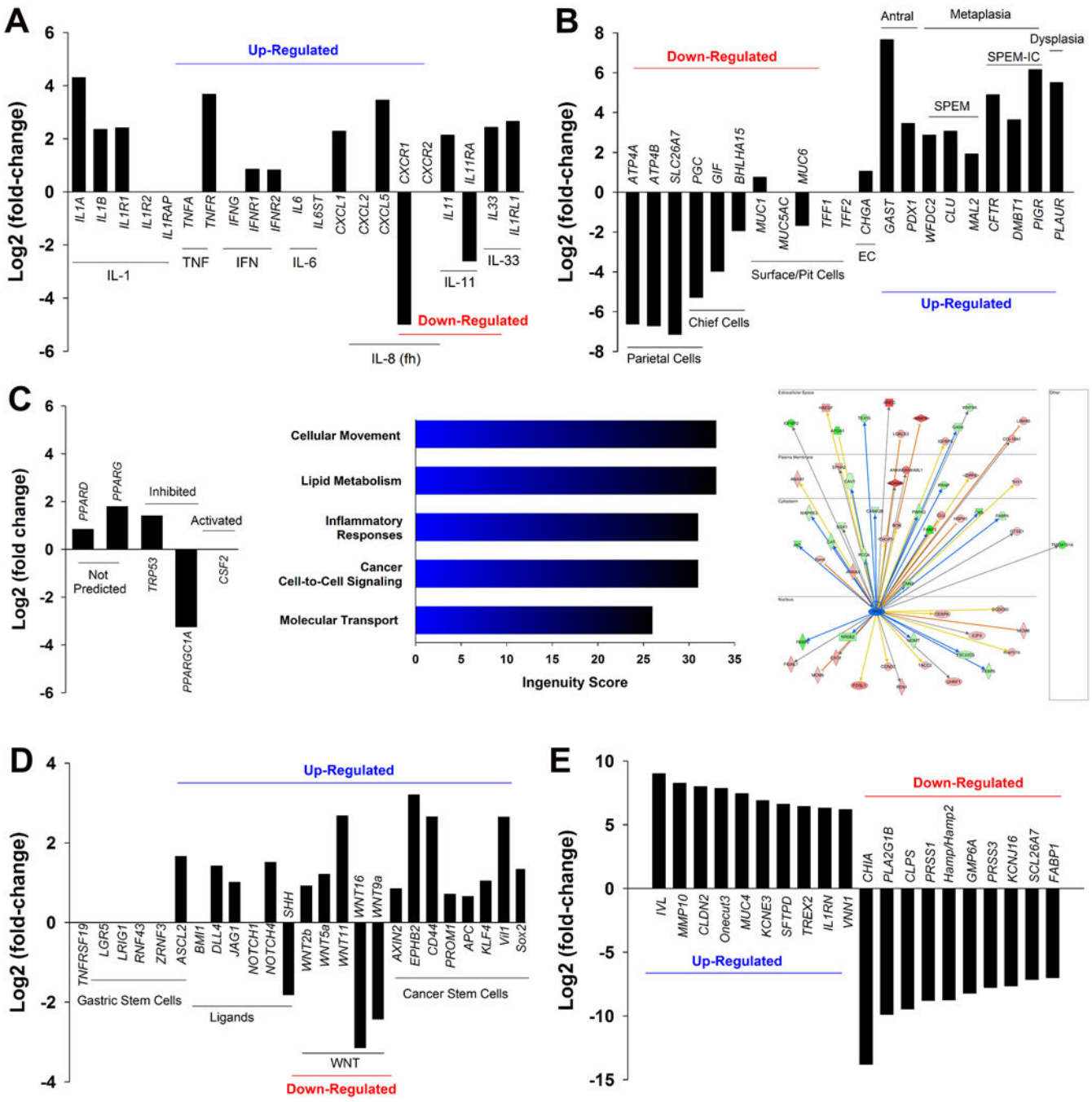

Figure 7.

Gene expression program in *CLDN18*DM at 7 weeks after birth is consistent with mucosal changes that promote gastric cancer development. All data were obtained from the RNAseq gene list; analysis was by Ingenuity Pathway Analysis (IPA). (*A*) Fold-change in cytokine gene expression levels. (*B*) Fold-change in differentiation markers including those of corpus and antral cell type-specific gene markers and metaplasia and dysplasia markers. (*C*) Fold-change in the expression of top pathway and network regulators identified from overall gene expression levels. IPA of *TP53* (p53) downstream gene expression levels. (*D*) Fold-change in

the expression of stem cell markers including surface markers for gastric stem cells, stem cell ligands, WNT signaling effectors, and cancer stem cells. (*E*) Fold-change in gene expression levels for the most highly up- and down-regulated genes. In all panels data are from $n = 3$ mice (male) each from WT and *CLDN18*DM. All data with black bars indicate significant gene changes with a *P*-value of 0.05 or less.